Nature Communications

https://doi.org/10.1038/s41467-026-69868-1

Article in Press

Self-driven recycling of spent Li-ion battery materials with electricity generation

Received: 9 June 2025

Accepted: 10 February 2026

Cite this article as: Huang, S., Huang, S., Li, M. *et al.* Self-driven recycling of spent Li-ion battery materials with electricity generation. *Nat Commun* (2026). https://doi.org/10.1038/s41467-026-69868-1

Shiqiang Huang, Songpeng Huang, Mengxiao Li, Hang Zhang, Xun Wang, Manohar Salla & Qing Wang

Self-driven recycling of spent Li-ion battery materials with electricity generation

Shiqiang Huang,[1,#] Songpeng Huang,[1,#] Mengxiao Li,[1] Hang Zhang,[1] Xun Wang,[1] Manohar Salla,[1] Qing Wang[1*]

[1]Department of Materials Science and Engineering, National University of Singapore, Singapore 117575, Singapore

[#]These authors contributed equally: Shiqiang Huang, Songpeng Huang

*e-mail: msewq@nus.edu.sg

Abstract

Spent lithium-ion batteries (LIBs) provide a valuable source of critical metals for cathode material production. However, the prevalent recycling technologies focus on processing only one type of spent cathode material, demanding high energy input and significant chemical consumption, which raises both environmental and economic concerns. Here, we propose a complementary redox-mediated recycling strategy for multiple types of spent cathode materials using a redox-targeting flow cell design. In this system, spent $LiFePO_4$ and layered oxide cathode materials serve as the anodic and cathodic feedstocks, respectively. Coupled redox-mediated oxidative and reductive leaching simultaneously generates electricity (theoretically 246 MWh per annum for 10,000 tonnes of black mass) while driving lithium-ion migration into the catholyte. Leaching efficiencies of critical metals exceed 95% for both materials, accompanied by a calculated carbon dioxide capture rate of 1,066 tonnes per annum. By integrating hydrogen looping for base and acid regeneration, the system operates over a closed loop without net chemical consumption. This strategy shows potential greater environmental and economic benefits compared with the traditional hydrometallurgical method based on techno-economic analysis, potentially offering a sustainable approach to LIBs recycling.

Introduction

Lithium-ion batteries (LIBs) have been dominating the battery market worldwide since their commercialization in 1991 for portable consumer electronics.[1] As the world strives for carbon-neutral energy solutions to meet greenhouse gas reduction targets, LIBs are now widely used in electric vehicles and large-scale energy storage systems.[2, 3] With such growing diversity of application scenarios, the global production capacity of LIBs is projected to rise sharply to 6.79 TWh by 2030, nearly quadrupling from 1.57 TWh in 2022.[4] And this increase in the production of LIBs creates significant pressure on the raw material market in the next decade due to limited natural supply and low metallurgical production capacity. Meanwhile, the accumulation of end-of-life LIBs has made their recycling an urgent priority from both resource and environmental

perspectives.[5, 6] On the other hand, spent cathodes of LIBs contain significantly higher concentrations of valuable metals, such as lithium (Li), cobalt (Co), nickel (Ni) and manganese (Mn), than those in mined ores and brine, making them a crucial source of raw materials.[7, 8] Therefore, designing a sustainable recycling process for spent cathodes is of great environmental, social and economic importance.[9, 10]

Pyrometallurgy and hydrometallurgy are two of the most established technologies for recycling spent cathodes and have been scaled up for industrial applications. In pyrometallurgy, spent cathodes are smelted at high temperatures of >1400 °C, producing a metal-based alloy (such as Co, Ni, and Cu) and lithium-containing slag, which requires further processing to extract the lithium.[11, 12] However, the high energy consumption and toxic gases emissions poses economic and ecological concerns. Hydrometallurgy operates at lower temperatures (<100 °C) using acid reagents to recover valuable metals such as Li, Co, Ni and Mn in the form of salt precursors. Nevertheless, the process consumes large amount of chemicals and generates wastewater, resulting in greater environmental impact.[13, 14] The recently reported direct regeneration technology provides a new direction for spent cathode recycling.[15] Instead of decomposition, extraction and resynthesis processes, the direct regeneration technology enables the replenishment of missing components in materials and thus the repaired materials can be used directly after regeneration.[16, 17] While the cost could in theory be reduced, the process requires high-quality raw materials, which may limit its scalability.[7, 18]

In addition, it is important to note that most existing recycling methods are limited to processing only one type of spent cathode material, which increases the investment and operational costs and lowers recycling efficiency.[19] Although upcycling strategies for mixed spent cathode materials has been reported to regenerate polyanionic and $LiNi_{1/3}Co_{1/3}Mn_{1/3}O_2$ cathode materials, it still requires energy input.[20-22] Spent cathode materials are not only valuable source of critical metals, they also contain significant amounts of free energy should there be a proper way of exploiting it, which however has so far been overlooked, leading to energy waste.

Thermodynamically, the potential difference between various spent cathode materials offers a promise for electricity generation. Here, we propose a complementary redox-mediated method to recycle multiple types of spent cathode materials while simultaneously harnessing the free energy stored in the waste materials. This strategy is broadly applicable, provided there is a sufficient potential difference between the spent cathode materials, with the lower-potential material undergoing oxidative leaching and the higher-potential material undergoing reductive leaching. Specifically, spent $LiFePO_4$ (LFP) and $LiNi_xMn_yCo_zO_2$/$LiCoO_2$ (NMC/LCO, $x+y+z \leq 1$) materials are used as the anodic and cathodic feedstocks in external tanks within a redox-targeting flow cell system.[23] During redox-mediated reactions, an electrochemical-chemical loop is established through the dissolved redox mediators shuttling between the electrodes and reactor tanks, enabling electron/hole transport and electricity generation (theoretically 246 MWh per annum for 10,000 tonne black mass). Following discharge, transition metal ions in the catholyte are recovered through precipitation in the form of metal hydroxides, while the accumulated Li^+ ions subsequently

capture CO_2 (1,066 tonnes per annum) to yield Li_2CO_3. The $FePO_4$ left in the anodic tank can be isolated and purified for the resynthesis of $LiFePO_4$.[24] The leaching efficiency of both spent LFP and NMC materials can reach as high as 95%. Additionally, a hydrogen-looping is integrated into the recycling system, enabling on-site acid and base regeneration, which eliminates the consumption of chemicals further lowering carbon footprint of the process. We anticipate that this closed-loop process offers a green, efficient, scalable and economical approach to LIBs recycling.

Results

Rational design of overall recycling process

The whole recycling process is depicted in Figure 1, with the cell architecture detailed in Figure S1. Step 1 involves leaching of the high-value metals in spent cathode materials with a redox-flow cell and producing electricity from the wastes. In this step, LFP and NMC (or LCO) black mass are loaded in the anodic and cathodic reactor tanks, with $[Fe(CN)_6]^{3-}$ and 2,4,5,6-tetrahydroxybenzene-1,3-disulfonic acid (THBDS) (Figure S2) acting as the anodic and cathodic redox mediators, respectively. The process operates through a chemical/electrochemical loop. On the anodic side, $[Fe(CN)_6]^{3-}$ is chemically reduced by LFP (equation 1) in the anodic reactor tank, with which Li^+ ions are released from the material. Along with Li^+ ions, the formed $[Fe(CN)_6]^{4-}$ in the anolyte flows back to the negative electrode compartment and loses electrons, which electrochemically regenerates $[Fe(CN)_6]^{3-}$ (equation 2) to complete a cycle. Meanwhile, Li^+ ions move to the positive electrode compartment across the cation-exchange membrane.

$$[Fe(CN)_6]^{3-} + LiFePO_4 \rightarrow [Fe(CN)_6]^{4-} + Li^+ + FePO_4 \quad (1)$$

$$[Fe(CN)_6]^{4-} - e^- \rightarrow [Fe(CN)_6]^{3-} \quad (2)$$

On the cathodic side, using $LiNi_{0.8}Mn_{0.1}Co_{0.1}O_2$ (NMC811) as an example, THBDS is chemically oxidized by NMC811 in the cathodic reactor tank generating $THBDS^{2+}$, with which Li^+, Ni^{2+}, Co^{2+}, and Mn^{2+} (equation 3) are leached in the presence of acid. $THBDS^{2+}$ in the catholyte then circulates back to the positive electrode compartment and gains electrons (equation 4), which electrochemically regenerates THBDS for the next cycle. Here acetic acid (HAc) is used for its good selectivity for high-value metals and acts as a buffer for a following H^+ regeneration process.[25]

$$0.5THBDS + LiNi_{0.8}Mn_{0.1}Co_{0.1}O_2 + 4H^+ \rightarrow 0.5THBDS^{2+} + Li^+ + 0.8Ni^{2+} + 0.1Co^{2+} + 0.1Mn^{2+} + 2H_2O \quad (3)$$

$$THBDS^{2+} + 2e^- \rightarrow THBDS \quad (4)$$

Both the $[Fe(CN)_6]^{3-/4-}$ and $THBDS^{2+}$/THBDS redox couples exhibit good stability (Figure S3 and S4) and can be reused in the recycling process. Accordingly, the overall reaction for the first step can be summarized as follows:

$$LiNi_{0.8}Mn_{0.1}Co_{0.1}O_2 + 4H^+ + LiFePO_4 \rightarrow 2Li^+ + 0.8Ni^{2+} + 0.1Co^{2+} + 0.1Mn^{2+} + 2H_2O + FePO_4 \quad (5)$$

The above process proceeds spontaneously ($\Delta G<0$) as a galvanic cell with continuous electricity production. Meanwhile, Li^+, Ni^{2+}, Co^{2+}, and Mn^{2+} are accumulated in the catholyte.

In Step 2, transition metal ions in the catholyte are separated via precipitation by adding NaOH, forming metal hydroxides ($M(OH)_2$, equation 6). In Step 3, CO_2 gas is then bubbled in the catholyte to separate Li^+ by forming Li_2CO_3 (equation 7). $M(OH)_2$ and Li_2CO_3 are the precursors for NMC811 synthesis.

$$2OH^- + 0.8Ni^{2+} + 0.1Co^{2+} + 0.1Mn^{2+} \rightarrow Ni_{0.8}Mn_{0.1}Co_{0.1}(OH)_2 \downarrow \quad (6)$$

$$2Li^+ + CO_2 + 2OH^- \rightarrow Li_2CO_3 \downarrow + H_2O \quad (7)$$

The first three steps effectively extract high-value metals with only H^+ and OH^- consumption (CO_2 gas is assumed to be from industrial waste, such as the flue gas). To ensure continuous recycling of spent cathode materials, H^+ and OH^- are regenerated through a hydrogen loop (Step 4). The hydrogen looping process is performed with two flow cells, designated as the HER cell and the HOR cell, which share a common catholyte from Step 3. In the HER cell, the anodic reaction involves the hydrogen evolution reaction (equation 8), accompanied by the regeneration of OH^-. The cathodic reaction involves the oxidation of THBDS (equation 9), during which cations such as Na^+ migrate through the membrane into the anolyte.

$$2H_2O + 2e^- \rightarrow H_2 + 2OH^- \quad (8)$$

$$THBDS - 2e^- \rightarrow THBDS^{2+} \quad (9)$$

While in the HOR cell, it features the anodic hydrogen oxidation reaction (equation 10) and cathodic reduction of $THBDS^{2+}$ (equation 11), during which H^+ ions migrate across the membrane into the catholyte, facilitating the regeneration of HAc.

$$H_2 - 2e^- \rightarrow 2H^+ \quad (10)$$

$$THBDS^{2+} + 2e^- \rightarrow THBDS \quad (11)$$

As the catholyte is shared between the two cells, the state of charge (SOC) of the $THBDS/THBDS^{2+}$ redox couple remains balanced. Consequently, the overall reaction for the hydrogen looping is effectively a water dissociation process (equation 12). The regeneration of H^+ and OH^- minimizes the consumption of acid and base in the leaching and precipitation steps.

$$H_2O \rightarrow H^+ + OH^- \quad (12)$$

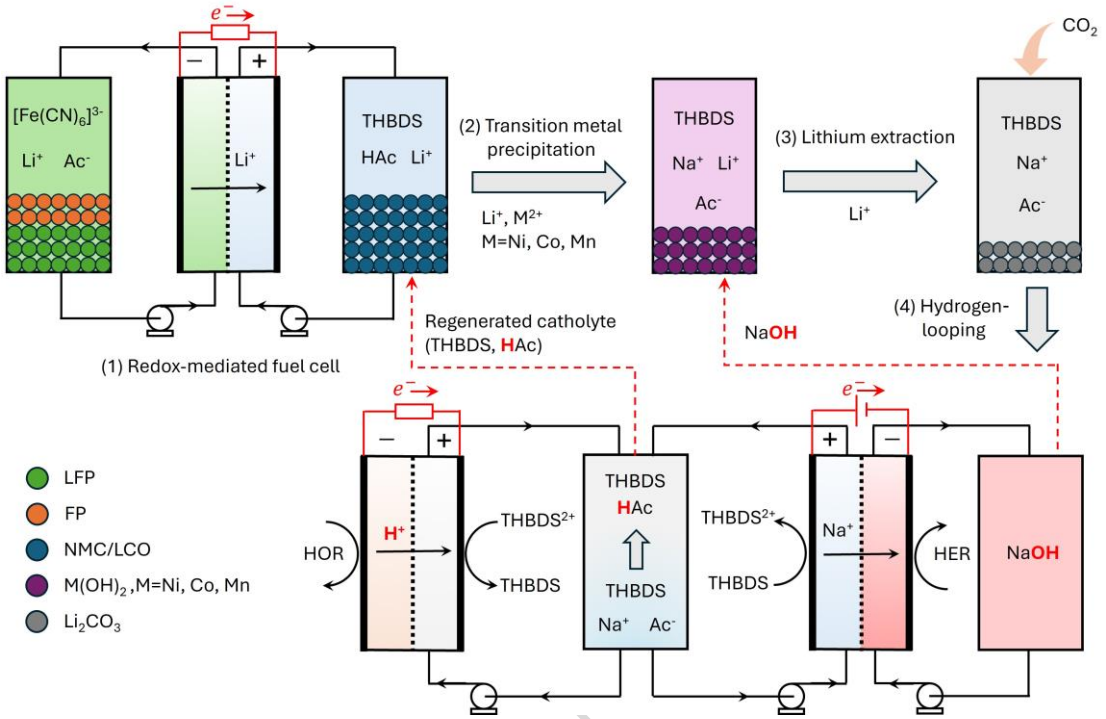

Figure 1. Schematic illustration of a sustainable redox-mediated spent LIB cathode materials recycling process. The system includes high-value metals leaching, transition metals separation, lithium recovery and base/acid regeneration. The high-value metals are extracted using a redox-targeting flow cell, where the spent cathode materials are used as the feedstock and redox active molecules serve as the mediators. The molecules shuttle between electrodes and reactor tanks, facilitating the transfer of electrons/holes through a chemical-electrochemical loop, while simultaneously generating electricity. The high-valued metals are accumulated in the catholyte during the continuous discharge process. The transition metal ions (M^{2+}) are separated via precipitation, forming metal hydroxides ($M(OH)_2$) and Li^+ captures CO_2 to produce Li_2CO_3. Both $M(OH)_2$ and Li_2CO_3 serve as precursors for synthesizing new cathode materials. To promote a sustainable recycling process with minimal chemical consumption and lower CO_2 emissions, base/acid regeneration occurs via a hydrogen looping process, where OH^- and H^+ are regenerated stepwise through a water-dissociation reaction, consuming only water. Cation-exchange membrane (CEM) was employed for all the flow cells.

Redox-mediated cathodic reaction

The redox-mediated reactions are central to the entire recycling process. Here we validate the cathodic reaction first. The equilibrium potential (E_{eq}) of NMC811 was monitored by the open circuit potential (OCP) and the half-wave potential ($E_{1/2}$) of THBDS was measured by cyclic voltammetry (CV). As shown in Figure 2a and S5, $E_{1/2}$ of THBDS is 0.60 V (*vs*. SHE) and the E_{eq} of NMC811 is 1.02 V (*vs*. SHE), resulting in a large driving force of 0.42 V for the reduction of

NMC811 by THBDS. The standard reduction potentials for Ni^{2+}, Co^{2+}, and Mn^{2+} deposition are -0.257 V, -0.280 V, and -1.185 V *vs*. SHE, respectively, which are significantly lower than the $E_{1/2}$ of THBDS. Therefore, under the experimental conditions, the deposition of these metal cations on the positive electrode is thermodynamically unfavourable and does not compete with the reduction of $THBDS^{2+}$. The redox-mediated reduction reaction of NMC811 by THBDS was subsequently verified by in situ UV-Vis spectroscopy with continuous monitoring of the absorbance changes of THBDS (see the setup in Figure S6). As shown in Figure S7, the THBDS solution exhibited no absorbance in the wavelength range of 350-600 nm. After the addition of NMC811, the absorbance in this range rapidly increased and eventually stabilized, indicating the progression of the continuous redox-mediated reduction reaction and the attainment of an equilibrium state. The corresponding concentration change of the THDBS was then calculated based on the standard calibration curve (Figure S8 and S9) to obtain kinetic information. Assuming it is a first-order reaction, the rate constant was calculated to be 0.0029 s^{-1} (Figure 2b). Thus, the redox-mediated reduction reaction has been validated from both thermodynamic and kinetic perspectives, and we then further demonstrated its feasibility in device.

The concentration changes of THBDS upon discharging was investigated by operando UV-Vis spectroscopy, where a spectro-electrochemical flow cell was constructed and connected to the cathodic flow channel outlet of a $[Fe(CN)_6]^{4-}$/$THBDS^{2+}$ flow cell (see the setup in Figure S8). For comparison, the UV-Vis spectra of the $THBDS^{2+}$ catholyte were first recorded at different durations of discharge without NMC811 solid materials in the external tank. The characteristic peak of $THBDS^{2+}$ at 376 nm gradually diminished with discharge process (Figure 2c), and a linear decrease in the absorbance at 380 nm was observed (Figure S10), both indicating the reduction of $THBDS^{2+}$. In stark contrast, when NMC811 was loaded in the reactor tank, a similar linear decrease in absorbance at 380 nm was observed initially, followed by a deviation from the linear trend during subsequent discharge, starting at around 15% state of discharge (SOD, Figure S10). It suggests the redox-mediated reduction reaction in the reactor tank was triggered. The regeneration of $THBDS^{2+}$ in the tank brings down the accumulation of THBDS and the redox-mediated reaction rate is able to match the electrochemical reaction rate, as evidenced by the stabilized absorbance between 40 and 80 minutes (Figure 2d). This redox-mediated cathodic reaction not only facilitates the leaching of Li^{+}, Ni^{2+}, Co^{2+}, and Mn^{2+} from NMC811 but also demonstrates significant potential for energy utilization, as evidenced by the capacity increase shown in Figure 2e.

An interesting observation during the discharge process was the red shift of the $THBDS^{2+}$ absorption peak from 376 nm to 450 nm (Figure 2d), suggesting the formation of a new compound with lower optical excitation energy than $THBDS^{2+}$.[26] Considering the gradual dissolution of M^{2+} ions and their potential to combine with ligands such as quinone-based molecules (Q) and HAc to form $(HAc)_m M^{2+}(Q)_n$ complexes (with m≥0 and n≥1), this red shift is likely due to an intramolecular charge transfer process within the $(HAc)_m M^{2+}(Q)_n$ complex.[27-30] As shown in Figure S11-13, the ex situ UV-Vis spectra of a mixed solution of $THBDS^{2+}$ and M^{2+} in 5 M HAc

solution exhibited a clear red shift, consistent with the operando experiments, indicating the formation of an $(HAc)_m M^{2+}(THBDS^{2+})_n$ complex. The structures of the complexes were further analysed with density functional theory (DFT) calculation (Figure S14 and Table S1-S4), which was identified as $Mn^{2+}(THBDS^{2+})_2$, $Co^{2+}(THBDS^{2+})_2$ and $(HAc)Ni^{2+}(THBDS^{2+})$ for Mn^{2+}, Co^{2+} and Ni^{2+}, respectively. During the subsequent discharge process, the absorption peak at 450 nm progressively vanished, indicating the further reduction of these intermediates and the formation of the final products, THBDS and M^{2+}. Therefore, the redox-mediated reduction reaction is not as straightforward as described by equations 3 and 4; it also involves the formation of intermediates and their subsequent reduction, as shown in equations 13 and 14.

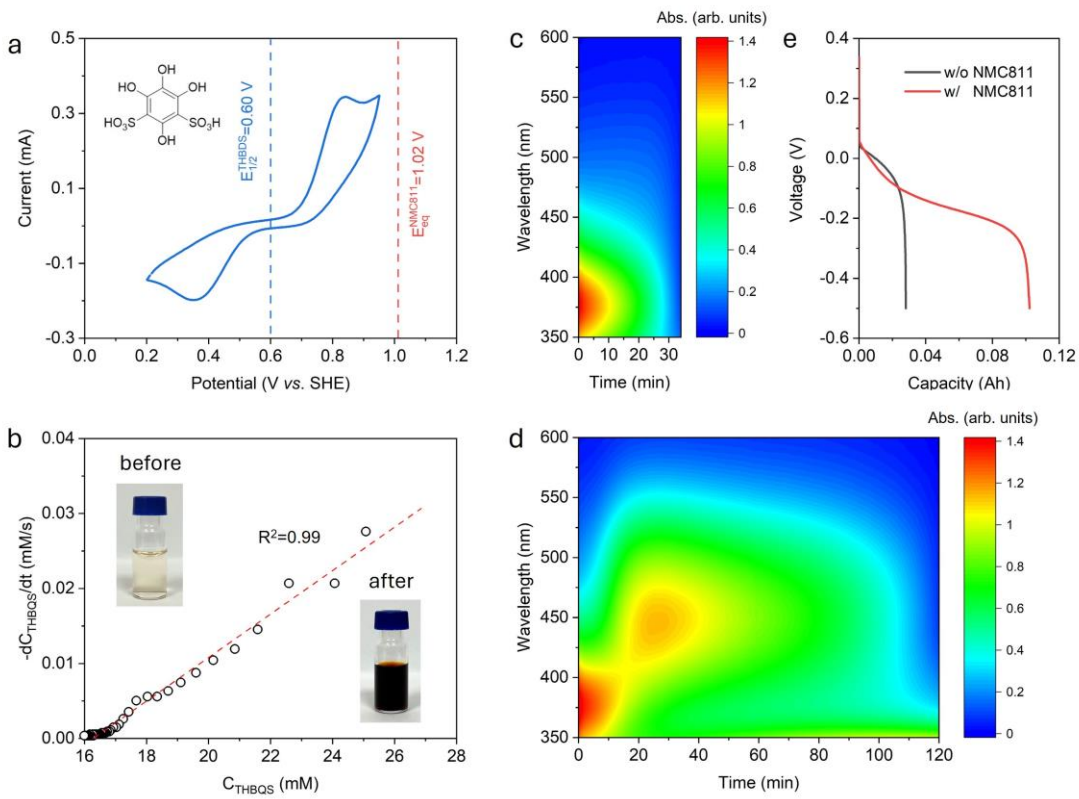

Figure 2. The redox-mediated reductive leaching process of NMC811. a, CV curve of THBDS and the equilibrium potential of NMC811 in 5 M HAc. The working electrode is a glassy carbon disk, and CV was conducted at a scan rate of 50 mV s^{-1} over a potential range of 0.2-0.95 V. Insert shows the molecular structure of THBDS. b, Concentration change *vs*. concentration plot of THBQS as obtained from in situ UV-Vis measurement. The reaction is assumed to be first-order and the rate constant is determined by the slope. Insert shows the colour changes of THBDS before and after reaction. The transparent THBDS became reddish after the reaction process. c-d, Operando UV-Vis spectra of catholyte of $[Fe(CN)_6]^{4-}$/$THBDS^{2+}$ flow cells without and with NMC811 loaded in the cathodic tanks during the discharge process. e, Corresponding voltage profiles of the $[Fe(CN)_6]^{4-}$/$THBDS^{2+}$ flow cells. The current density was 10 mA cm^{-2}.

$$nTHBDS^{2+} + M^{2+} + mHAc \rightarrow (HAc)_m M^{2+}(THBDS^{2+})_n \quad (13)$$

$$(HAc)_m M^{2+}(THBDS^{2+})_n - 2ne^- \rightarrow nTHBDS + M^{2+} + mHAc \quad (14)$$

We not only tested NMC-based cathode materials but also evaluated the universality of the redox-mediated cathodic reaction using LCO feedstock. As shown in Figure S15, the E_{eq} of LCO is 0.98 V (*vs*. SHE), so the driving force of the reaction can reach around 0.38 V. The reaction rate constant was calculated to be 0.0018 s^{-1} based on in situ UV-Vis spectra (Figure S16). The smaller rate constant of LCO compared to NMC811 may partly be due to smaller driving force. In addition, the similar ionic radii of Ni^{2+} and Li^+ could also affect the reaction rate, as Li^+/Ni^{2+} disorder reduces structural stability, leading to faster reaction kinetics in NMC811 than in LCO.[25] It was also demonstrated during the operando experiment with a $[Fe(CN)_6]^{4-}/THBDS^{2+}$ flow cell, where no stable concentration plateau appeared throughout the discharge process (Figure S17), indicating that while the redox-mediated reaction slows down the accumulation of THBDS, the reaction rate cannot keep up with the electrochemical reaction rate at the same current density. Additionally, a red shift in the absorbance peak and its subsequent disappearance were also observed in the operando UV-Vis spectra (Figure S18), suggesting a similar reaction process involving the formation of $Co^{2+}(THBDS^{2+})_2$ intermediates. Overall, the redox-mediated reduction process proceeds with two parallel reaction pathways: the initial direct reduction of NMC/LCO with a chemical/electrochemical loop (equations 3 and 4) and the subsequent reduction of intermediates (equations 13 and 14). The reaction concludes with the complete reduction of $THBDS^{2+}$ to THBDS, accompanied by the leaching of Li^+ and M^{2+} from solid materials into solution, meanwhile with electricity production.

Redox-mediated anodic reaction

The anodic reaction was investigated using $[Fe(CN)_6]^{3-/4-}$ as a redox mediator. $E_{1/2}$ of $[Fe(CN)_6]^{3-/4-}$ was tested to be 0.47 V (*vs*. SHE) by CV, while the E_{eq} of LFP was 0.43 V (*vs*. SHE), as determined by OCP measurements (Figure 3a and Figure S19). This yields a driving force of 0.04 V for the redox-mediated oxidation reaction. Additionally, the kinetic information was obtained by monitoring the OCP changes of $[Fe(CN)_6]^{3-}$ solution throughout the redox-mediated process with excessive LFP (Figure S20). The concentration of $[Fe(CN)_6]^{3-}$ was determined based on the Nernst equation.

$$E = E_{1/2} + \frac{RT}{F}\ln\left(\frac{C_{[Fe(CN)_6]^{3-}}}{C_{[Fe(CN)_6]^{4-}}}\right) \quad (15)$$

where *T* is temperature, *R* is the gas constant, and *F* is the Faraday constant. And we assume $E_{1/2}=E_f$, where E_f is the formal potential, and it is a first-order reaction. Further by plotting the concentration changes *vs*. concentration, the rate constant was calculated to be 0.093 s^{-1} (Figure 3b).

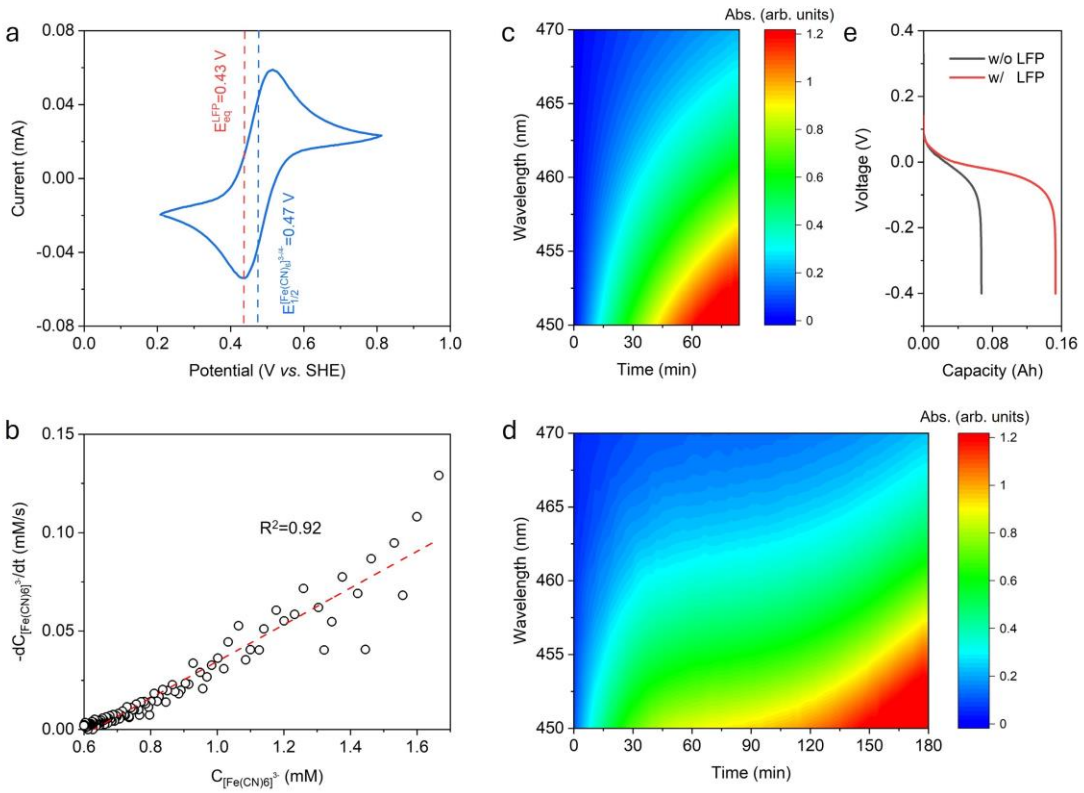

Figure 3. The redox-mediated oxidative leaching process of LFP. a, CV curve of $[Fe(CN)_6]^{3-/4-}$ and the equilibrium potential of LFP in 3 M LiAc. The working electrode is a glassy carbon disk and CV was conducted at a scan rate of 50 mV s^{-1} over a potential range of 0.2-0.8 V. b, Concentration change *vs*. concentration plot of $[Fe(CN)_6]^{3-}$ as obtained from OCP measurement. The reaction is assumed to be first-order and the rate constant is determined by the slope. c-d, Operando UV-Vis spectra of anolyte of $[Fe(CN)_6]^{3-/4-}$-based symmetric flow cells without and with LFP loaded in the anodic tanks during the discharge process. e, Corresponding voltage profiles of the $[Fe(CN)_6]^{3-/4-}$-based symmetric flow cells. The current density was 10 mA cm^{-2}.

To verify the reaction mechanism with respect to the concentration evolution upon operation, operando UV-Vis measurements were performed with $[Fe(CN)_6]^{4-/3-}$-based symmetric cells (Figure S21). The UV-Vis spectra of the anolyte in the absence of LFP were recorded at different durations of discharge (Figure 3c), from which a linear relationship between the absorbance at 460 nm (Figure S22) and time can be used as a reference to calibrate the calculations of $[Fe(CN)_6]^{3-}$ concentration. In the presence of LFP in the anodic tank, the UV-Vis spectra initially resemble those observed without LFP in the first 15 minutes (around 18% DOD), showing a linear increase at 460 nm, indicating the electrochemical oxidation of $[Fe(CN)_6]^{4-}$. Subsequently, the concentration changes of $[Fe(CN)_6]^{3-}$ slow down, signalling the onset of a redox-mediated reaction between $[Fe(CN)_6]^{3-}$ and LFP (Figure S22). During the subsequent discharge process, the

accumulation of $[Fe(CN)_6]^{3-}$ in the anolyte increases the equilibrium potential, creating sufficient driving force for the oxidation of LFP. As a result, the redox-mediated reduction rate of $[Fe(CN)_6]^{3-}$ in the anodic tank balances the electrochemical oxidation rate of $[Fe(CN)_6]^{4-}$ at the electrode, leading to a steady state with nearly unchanged concentration observed between 45 and 135 minutes (Figure 3d). By the end of the discharge process, with adequate reaction of LFP, all $[Fe(CN)_6]^{4-}$ was oxidized to $[Fe(CN)_6]^{3-}$. The concentration of $[Fe(CN)_6]^{3-}$ determined along with the discharge process was in consistence with the voltage profiles (Figure 3e) of the same cell. It is observed that during the discharge process, the cell without LFP loaded in the tank initially shared similar voltage changes to the cell with LFP before its voltage started to drop more steeply and diverge from the latter.

Concept verification

With successful demonstrations of the redox-mediated reactions at both the cathodic and anodic directions, a redox-targeting flow cell was fabricated for concurrent leaching of spent LFP and NMC. As shown in Figure 4a, the $[Fe(CN)_6]^{4-}$/$THBDS^{2+}$ flow cell, equivalently loaded with 1.15 g of NMC811 in the cathodic tank (77 g/L) and 1.99 g of LFP in the anodic tank (74 g/L), achieved a discharge capacity of 0.215 Ah (67% utilization) and generated 0.031 Wh of electricity. And the concentrations of Li^+, Ni^{2+}, Co^{2+} and Mn^{2+} in catholyte were determined using an inductively coupled plasma-optical emission spectrometer (ICP-OES), which were 1.210 M, 0.481 M, 0.063 M, and 0.057 M, respectively. The molar ratio of Ni^{2+}, Co^{2+} and Mn^{2+} was approximately 8:1:1, aligning with the nominal molar ratio of NMC811. The corresponding leaching efficiencies of Li^+, Ni^{2+}, Co^{2+} and Mn^{2+} were calculated to be 75%, 75%, 78%, and 71%, respectively. During the discharge process, the cathodic reaction gradually consumed H^+, leading to an increase in pH. This pH shift in the environment creates a larger driving force for the redox-mediated reduction process by lowering the potential of the $THBDS^{2+}$/THBDS redox couple, as illustrated in the Pourbaix diagram (Figure S23). However, the diminishing H^+ concentration in the catholyte adversely affects the reaction kinetics and leaching efficiency.[31] So it is important to figure out the rate-limiting step for the cathodic reaction, which could be either interfacial electron transfer process or H^+ involved reactions.[31-34]

Given that the cathodic reaction operates as an electrochemical/chemical loop, achieving high material utilization requires balancing the kinetics of the electrochemical and chemical reactions. To investigate this, we tested material utilization at varying current densities (electrochemical reaction rates) at 77 g/L NMC811 loading in tank. As shown in Figure S24, the utilization was around 55% and 61% at the current density of 1 mA cm^{-2} and 10 mA cm^{-2}, respectively. Reducing the current density (i.e., slowing the electrochemical reaction rate) does not lead to a significant increase in utilization, which suggests that the interfacial electron transfer rate of the chemical reaction is sufficiently fast to match the electrochemical reaction rate, and the H^+ involved reactions could be the rate-limiting step. Interestingly, at a lower current density of 1 mA cm^{-2}, multiple discharge plateaus were observed, indicating gradual pH changes in the catholyte. In contrast, at higher current densities (5 mA cm^{-2} and 10 mA cm^{-2}), only a single discharge plateau

was present, suggesting a stable pH environment during the discharge process. The rapid reaction rate of the redox-mediated chemical process likely facilitates the dissociation of HAc, with the balance between consumption and dissociation maintaining a stable pH environment. However, as H^+ is gradually consumed in the catholyte, a decrease in H^+ concentration can affect the reaction rate, leading to relatively low utilization of NMC811. So, the utilization of HAc (or the termination pH) is critical for achieving a high leaching efficiency. To optimize the reaction, increasing the supply of H^+ or lowering the NMC/HAc ratio enables higher NMC leaching efficiency. Based on the leaching efficiencies of 71-78% and the testing conditions of NMC811/HAc = 0.79 mol / 5 mol, it's estimated that 0.561-0.616 mol of NMC811 was reacted, which consumed 2.244-2.464 mol of HAc, corresponding to an HAc utilization of 45%-49%. Applying the Henderson-Hasselbalch equation:

$$pH = pK_a + lg\frac{[Ac^-]}{[HAc]} \quad (15)$$

With pK_a(HAc) = 4.76, the termination pH is calculated to be 4.671-4.747.

Assuming an HAc utilization of 45%, 1 L 5 M HAc provides a minimum H^+ supply of 2.250 mol, corresponding to 54 g of NMC811. Based on this critical value, we lowered the NMC811/HAc ratio to 5.1 g/L (0.053 mol / 2.250 mol), achieving a utilization of 92% (Figure S25), which confirmed the validity of the proposed mechanism. This suggests that the rate-limiting step of the redox-mediated cathodic reaction is governed by the H^+ concentration, which depends on the total acid concentration and the H^+ dissociation rate in the electrolyte. Consequently, there exists a trade-off between material utilization and proton consumption in the cathodic reaction. On the other hand, pH-independent anodic reaction can achieve a high utilization of around 95% (Figure S26 and S27). Given that the redox-mediated anodic reaction proceeds at a significantly faster rate than the cathodic reaction (0.093 s^{-1} vs. 0.0029 s^{-1}), higher utilization of LFP was achieved across a range of applied current densities (Figure S28) compared with NMC811. Therefore, the cathodic reaction constitutes the primary bottleneck of the overall system.

It is worth noting that the active materials (NMC811 and LFP) were employed in the form of granules, fabricated from NMC811/LFP powders mixed with carbon black and PVDF binder, thereby intentionally incorporating the carbonaceous and polymeric components characteristic of real black mass. These additives exerted negligible influence on the process performance, as reflected in the high utilization of both NMC811 and LFP. For trace amount of metallic impurities which may present in the black mass, they are dissolved alongside the cathode materials during the leaching step and can be removed via pH adjustment, solvent extraction, electrolysis, ion exchange, or membrane filtration.[35, 36] This study focuses on the redox-mediated chemistries and closed-loop design for complementary spent cathode materials recycling, while impurity treatment represents a broader and equally important challenge in battery recycling that lies beyond the primary scope of this study.

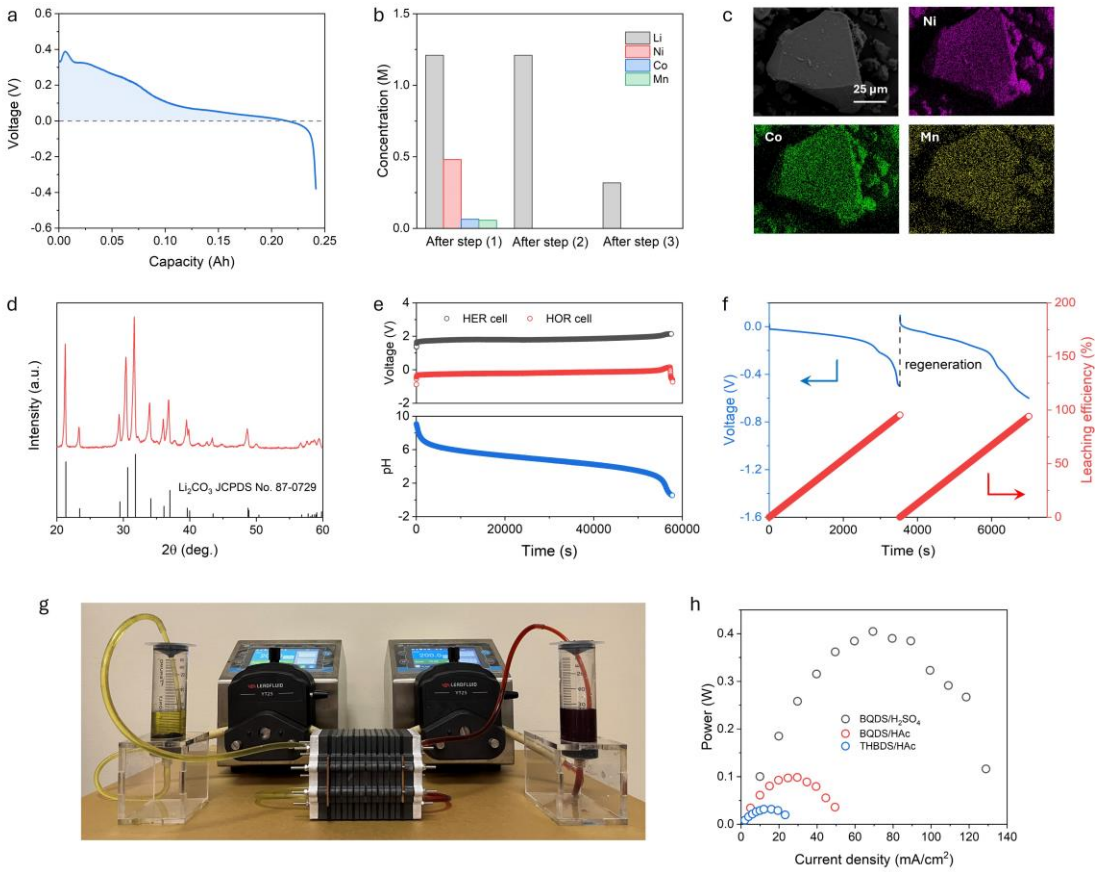

Figure 4. Complementary redox-mediated spent cathode materials recycling. a, Voltage profile of a $[Fe(CN)_6]^{4-}$/$THBDS^{2+}$ flow cell with LFP loaded in the anodic reactor tank and NMC811 in the cathodic reactor tank. The current density is 10 mA cm^{-2} and voltage profile is plotted with IR correction. b, Concentrations of Li^+, Ni^{2+}, Co^{2+} and Mn^{2+} in catholyte after each step. c, SEM image of $Ni_{0.806}Mn_{0.1}Co_{0.11}(OH)_2$ with the corresponding elemental mapping results of Ni (purple), Co (green) and Mn (yellow). d, XRD pattern of the Li_2CO_3 product. e, Voltage profiles of the HER and HOR cells during the hydrogen looping processes and the corresponding pH changes of the THBDS-based electrolyte. For the HER cell, catholyte was THBDS solution and anolyte was 0.1 M NaOH solution. Pt was used as the HER catalysts. The current density was 50 mA cm^{-2}. For the HOR cell, THBDS solution was used catholyte and H_2 gas was supplied to the negative electrode. Pt/C was used as the HOR catalysts. The current density was 50 mA cm^{-2}. f, Voltage profiles of the $[Fe(CN)_6]^{4-}$/$THBDS^{2+}$ flow cell after *ex-situ* leaching process and the corresponding leaching efficiency calculated based on the discharge capacity. g, The optical image of the $[Fe(CN)_6]^{4-}$/$THBDS^{2+}$ flow cell stack constructed by six single cells with NMC811 loaded in the cathodic tank and LFP in the anodic tank. h, Power vs. current density curve of the flow cell stacks. The catholytes was 35 mL 0.1 M THBDS/5 M HAc/1 M KCl or 35 mL 0.1 M BQDS/5 M HAc/1 M KCl or 35 mL 0.1 M BQDS/H_2SO_4, and the anolyte was 35 mL 0.2 M $Li_3Fe(CN)_6$/3 M LiAc. Excessive NMC811 and LFP were loaded in the cathodic and anodic tanks, respectively.

To separate Li^+, Ni^{2+}, Co^{2+} and Mn^{2+} in the leachate, a co-precipitation process was carried out after the initial step. While Li^+ ions remained in solution, nearly all the Ni^{2+}, Co^{2+} and Mn^{2+} were recovered as $Ni_xMn_yCo_z(OH)_2$, with their concentrations reduced to the 10^{-5} M level (Figure 4b). Elemental analysis revealed the precipitated metal hydroxide has a composition of $Ni_{0.806}Mn_{0.1}Co_{0.11}(OH)_2$. Additionally, scanning electron microscope (SEM) image and energy-dispersive spectroscopy (EDS) elemental maps confirmed a uniform distribution of Ni, Co, and Mn elements within individual particles (Figure 4c). X-ray diffraction (XRD) patterns for the $Ni_{0.806}Mn_{0.1}Co_{0.11}(OH)_2$ powders is shown in Figure S29, which is similar to that of pure β-$Ni(OH)_2$.[37] All diffraction lines were indexed to a hexagonal structure with a space group of $p\bar{3}m1$, indicating that Co^{2+} and Mn^{2+} partially substituted for Ni^{2+} in the $Ni(OH)_2$ lattice to form a solid solution.

With sufficient removal of Ni^{2+}, Co^{2+} and Mn^{2+} from the leachate, CO_2 gas was then bubbled in the Li^+-rich solution to produce lithium carbonate (Li_2CO_3) precipitate which was confirmed by the XRD and SEM as shown in Figure 4d and Figure S30, respectively. Although the concentration of CO_2 affects the reaction rate (Figure S31), Li_2CO_3 could eventually be obtained as the final product after sufficient reaction time (Figure S32). As a result, the obtained materials can serve as the raw materials for NMC811 synthesis.

The strategy is also used for LCO recycling. As shown in Figure S33, similar to using NMC811 as the cathodic feedstock in a $[Fe(CN)_6]^{4-}$/$THBDS^{2+}$ flow cell, multiple voltage plateaus were observed at a low current density of 1 mA cm^{-2} while only a single discharge plateau appeared at a higher current density (5 mA cm^{-2} and 10 mA cm^{-2}) with LCO loaded in the cathodic tanks. This indicates that a fast reaction rate promotes the dissociation of HAc, which is similar to that observed with NMC811. The appearance of multiple voltage plateaus at lower current densities suggests that acid dissociation is the rate-limiting step, as the electron transfer rate on electrode and in the external cathodic tank remained balanced. However, the utilization of LCO gradually decreased from 50% to 38% as the current density increased, suggesting that at a higher current density of 10 mA cm^{-2}, the rate-limiting step shifted from acid dissociation to the interfacial electron transfer process. This behavior differs from that observed with NMC811 and may be attributed to a slower rate constant (0.0029 s^{-1} *vs*. 0.0018 s^{-1}). Based on the analysis, with sufficient H^+ supply and a balanced electron transfer rate between electrochemical and chemical reactions, a higher leaching efficiency of 87% was achieved (Figure S34) in one round of leaching. Subsequently, Co^{2+} was precipitated as $Co(OH)_2$ and Li^+ reacted with CO_2 gas to form Li_2CO_3 (Figure S35).

After recovering all valuable metal elements, the catholyte became weakly alkaline. To establish a sustainable closed-loop recycling process, a hydrogen looping was implemented to regenerate the acidic environment of the used catholyte while producing base for subsequent precipitation. The hydrogen looping was designed based on a flow battery setup, as illustrated in Figure 1 (Step 4) and described in equations 8-12. The pH changes of the used catholyte were monitored in real time during the reaction. Initially, the pH was around 9. As the HOR reaction progressed, the pH

rapidly dropped to approximately 7, indicating that H^+ generated in the HOR cell were effectively transferred to the catholyte, reducing its pH. Subsequently, a slower rate of pH change was observed between 7 and 3, attributed to the buffering effect of Ac^-, which captures H^+ to form HAc in the catholyte. At the end of the reaction, the pH decreased rapidly to around 1, confirming the complete regeneration of the acidic catholyte. The Faradaic efficiency of the whole reaction process was determined to be around 98.8% by the cation (Li^+, Na^+ and K^+) changes in the used catholyte (Figure S36). Due to the inaccuracy of the pH meter at extremely high OH^- concentrations, the OH^- concentration for the anolyte in the HER cell is estimated based on cation exchange. After hydrogen looping, it was approximately 5.04 M, resulting in an estimated anolyte pH of ~14.7. The charge voltage of the HER cell was approximately 1.79 V, while the discharge voltage of the HOR cell was about -0.19 V, resulting in an overall voltage of 1.98 V for hydrogen looping. Note the theoretical charge and discharge voltages are around 1.40 V and 0.60 V for the HER and HOR cells, respectively, indicating an overpotential of 0.39 V for the HER cell and 0.79 V for the HOR cell. The significant polarization, particularly in the HOR cell, is attributed to the large internal resistance of the devices. The structure of these cells should be optimized to enhance the energy efficiency.

With successful demonstration of the closed-loop recycling process, we proceeded to validate the concept using NMC622 and LFP black mass. Following the completion of the redox-mediated leaching reactions between THBDS and NMC622, as well as $Li_3[Fe(CN)_6]$ and LFP, the resulted $THBDS^{2+}$/THBDS and $Li_3[Fe(CN)_6]$/$Li_4[Fe(CN)_6]$ solutions were employed as the catholyte and anolyte, respectively, in the flow cell. Notably, the THBDS in the catholyte and $Li_3[Fe(CN)_6]$ in the anolyte did not contribute to the cell capacity. Instead, the capacity was originated from $THBDS^{2+}$ and $Li_4[Fe(CN)_6]$, which were products of the redox-mediated reactions with the waste materials. In other words, the discharge capacity was provided by NMC622 and LFP. Consequently, the leaching efficiency was estimated based on the discharge capacity, which was approximately 95% for the first recycling process (Figure 4f). To have a more accurate results, the leaching efficiency of metal ions were determined by elemental analysis, which were 99%, 98.3%, 98% and 99% for Li^+, Ni^{2+}, Co^{2+} and Mn^{2+}, respectively. The deviation in leaching efficiency may be attributed to incomplete utilization of the electrolytes in the cell, which leads to an underestimated leaching efficiency. The THBDS-based catholyte was regenerated using a hydrogen looping with no obvious capacity decay (Figure S37) and reused in the subsequent recycling process. The leaching efficiency, calculated based on the discharge capacity, was 94% (Figure 4f). Elemental analysis revealed the leaching efficiencies of Li^+, Ni^{2+}, Co^{2+}, and Mn^{2+} to be 97%, 96%, 95.2%, and 97%, respectively, indicating good leaching capability of the electrolytes.

The THBDS/$Li_3[Fe(CN)_6]$ single cell exhibited a low voltage when using HAc as the supporting electrolyte. To evaluate its power performance, a battery stack (Figure 4g) consisting of six single cells was constructed. With an excess of NMC811 and LFP loaded in the external tanks, the stack voltage reached 0.92 V (Figure S38) and achieved a peak power of 0.032 W (Figure 4h). Given that the cell voltage is determined by the potentials of the catholyte and anolyte, 4,5

dihydroxybenzene-1,3-disulfonic acid (BQDS), with a higher $E_{1/2}$, was used to replace THBDS as the catholyte (Figure S39). The BQDS/$Li_3[Fe(CN)_6]$ stack with HAc as the supporting electrolyte demonstrated an improved peak power of 0.099 W. Considering that the $E_{1/2}$ of BQDS is pH-dependent (Figure S40), H_2SO_4 was subsequently used as the supporting electrolyte to further enhance power performance, resulting in a significantly higher peak power of 0.40 W. It is also noteworthy that BQDS exhibits fast reaction kinetics, as indicated by a smaller peak separation (Figure S39) when H_2SO_4 is used as the supporting electrolyte, which further contributes to the enhanced power performance. Nevertheless, the stability of BQDS is inferior to that of THBDS (Figure S41), which is caused by the Michael reaction and nucleophilic addition of water.[38] Thus, for practical implementation, optimal redox mediators for the cathodic reaction should exhibit high stability, matched redox potential, and rapid reaction rate.

Techno-economic analysis

A techno-economic analysis (TEA) by comparing the traditional hydrometallurgical (Hydro) recycling with our complementary redox-mediated recycling was performed using the EverBatt 2023 model. The compositions of NMC811 and LFP black mass are detailed in Figure S42, based on data from the model. The NMC811 black mass contains 57.8% NMC811 active materials, while the LFP black mass comprises 64.6% LFP active materials. And 1 kg of black mass consisting of 0.236 kg NMC811 and 0.382 kg LFP was used for the cost analysis.

To simplify the recycling processes, we focus on the extraction of valuable elements and the use of various key reagents (Figure 5a, 5b, Table S5-S7). Thus, the conventional H_2SO_4/H_2O_2 leaching method are used for both NMC811 and LFP in Hydro process.[10, 39] Both NMC811 and LFP are fully leached initially. For LFP, lithium is recovered as Li_2CO_3 by adding Na_2CO_3. For NMC811, Ni^{2+}, Mn^{2+}, and Co^{2+} are co-precipitated as $Ni_xMn_yCo_z(OH)_2$ precursors by adjusting the solution pH, after which lithium is recovered from the remaining solution as Li_2CO_3 using Na_2CO_3. Based on the corresponding chemical equations, the H_2SO_4, H_2O_2, NaOH and Na_2CO_3 used for NMC811 spent cathode are 0.357 kg, 0.041 kg, 0.194 kg and 0.128 kg, respectively. And H_2SO_4, H_2O_2 and Na_2CO_3 used for LFP spent cathode are 0.119 kg, 0.041 kg and 0.128 kg, respectively. The overall consumption of H_2SO_4, H_2O_2, NaOH and Na_2CO_3 for 1 kg black mass are 0.476 kg, 0.082 kg, 0.194 kg and 0.256 kg. In contrast, for the redox-mediated recycling process, the redox mediators are assumed to remain stable throughout the operation, with negligible consumption. Over a 10-year period, the total requirement per kilogram of black mass is only 7.5×10^{-5} kg THBDS and 1.5×10^{-4} kg $Li_3Fe(CN)_6$, which can be considered insignificant. The only net reactants consumed are H^+ and OH^-, which are continuously regenerated via the hydrogen looping process, with an associated electricity demand of 0.494 kWh per kilogram of black mass. In the redox-mediated recycling process, HAc was used as the proton source for leaching, while Ac^- served as the buffering agent to capture proton and regenerate HAc during the hydrogen-looping step. As a result, no SO_4^{2-} species are involved, and the Na^+ ions are converted to NaOH within the loop, eliminating

the need for specific Na_2SO_4 management. Regarding off-gas and evaporation effects, although the redox-mediated system operates under a sealed or closed-loop configuration, minor off-gas and evaporation phenomena are still considered for completeness. Off-gas effects mainly originate from internal pressure balancing, gas recirculation, and trace hydrogen handling within the loop, while evaporation losses are attributed to limited solvent volatilization or temperature-driven vapor-condensate cycling. These contributions were included as low-level utility duties in the TEA, consistent with comparable large-scale flow-battery and hydrometallurgical assessments, and have little influence on the overall cost trends.

Unit-cost breakdowns are summarized in Figure 5c, Figure S43, Table S8 and S9. In both recycling processes, the annual capital cost is a dominant factor, accounting for 44.3% of the total cost in the redox-mediated recycling process and 50.6% in the Hydro process. The material cost in the redox-mediated strategy is relatively low (2.5% of total) because the redox mediators serve as both reducing and oxidizing agents and are regenerated during operation. Additionally, acids and bases are produced in situ via the hydrogen looping process, which primarily consumes electricity. By contrast, in Hydro recycling, the purchase of acid/alkaline reagents and salts makes materials a much larger contributor (17.5% of total). On the other hand, due to higher electricity usage for the hydrogen looping, the utility cost is significantly greater for the redox-mediated process than for the Hydro process (15.3% vs. 2.9%). Accounting for potential flow cell leakage and membrane fouling, the maintenance cost of the redox-mediated process is slightly higher than that of the Hydro process (11.7% vs. 8.3%). Overall, the recycling costs of redox-mediated and Hydro processes are \$1.07 and \$1.62 per kilogram of feedstock, respectively. The final products obtained from both methods are the same: Li_2CO_3 and $M(OH)_2$. Assuming that all the recycling products would be used for re-synthesis, the revenue generated was \$4.26 per kilogram of feedstock, resulting in a profit of \$3.18 per kilogram for the complementary redox-mediated method and \$2.64 per kilogram for the Hydro method (Figure 5d). To evaluate the robustness of the techno-economic results, sensitivity and uncertainty analyses were performed by varying key parameters for the redox-mediated method, including mediator loss (0-2%/cycle), overpotentials/internal resistance (±20%), electricity price (±30%), utilization of black mass (70-100%), and feed-composition variability (±20%). As summarized in Figure S44, the profit decreased slightly from \$3.19/kg to \$3.16/kg with a mediator loss of 2%/cycle. Variation in overpotential/internal resistance (±20%) resulted in profits ranging from \$3.14/kg to \$3.22/kg, while changes in electricity price (±30%) produced a range of \$3.13/kg to \$3.23/kg. In contrast, the profitability was more sensitive to black mass utilization, ranging from \$1.91/kg to \$3.19/kg, and to feed-composition variability, which yielded profits between \$2.34/kg and \$4.04/kg. These results indicate that the overall economics are primarily influenced by the utilization efficiency of the black mass and the variability of feed composition, whereas the effects of mediator loss, overpotential, and electricity cost are comparatively moderate.

Furthermore, the complementary redox-mediated method is able to produce electricity during the first step. Considering a recycle plant annually processes 10,000 tonnes of black mass, it comprises

2,358 tonnes of NMC811 and 3,824 tonnes of LFP. With the plant operating 320 days per annum, the daily processing rates for NMC811 and LFP are 7.37 tonnes (75,756 mol) and 11.95 tonnes (75,756 mol), respectively. Based on the data in Figure 4a, with a 67% utilization of the solid materials, the plant generates approximately 196 kWh of electricity per day. Over a 10-year operational period, this corresponds to a total electricity output of 0.63 GWh (Figure 5e). When employing a redox mediator with a higher redox potential, such as BQDS, a higher discharge voltage can be achieved, thereby increasing the overall electricity production (Figure S45). Under these conditions, the theoretical electricity generation reaches 246.4 MWh per annum, resulting in a total of 2.46 GWh over ten years. Consequently, the projected electricity generation over a 10-year period lies within the range of 0.63-2.46 GWh. Additionally, regardless of the redox mediators used in the catholyte, CO_2 capture presents another contributing factor. Considering 67%-100% utilization of active materials in the black mass, the CO_2 capture rate is 2.23-3.33 tonnes per day. Over ten years, the total CO_2 capture is estimated to be 7,140-10,656 tonnes (Figure 5e). In addition, our complementary redox-mediated strategy demonstrated the feasibility of concurrently recycling two types of spent cathode materials. As a result, compared with Hydro method, the complementary redox-mediated approach offers significant advantages in terms of cost efficiency, profitability, co-recycling feasibility, environmental sustainability, and energy savings (Figure S46).

Looking forward, several aspects still require further development before large-scale deployment can be achieved. For example, redox mediator stability remains a critical challenge, as they may undergo gradual degradation over extended operation; this calls for the rational design of next-generation RMs with optimized potentials and long-term durability. The high cost associated with Nafion membranes can be alleviated by employing alternatives such as sulfonated poly(ether ether ketone) (SPEEK) membranes (Figure S47), thereby further lowering the fixed cost.[40] Similarly, the hydrogen-looping subsystem must be refined through advances in flow field engineering, catalyst design, and low-resistance membranes to minimize overpotentials and further improve energy efficiency. In addition, system-level integration needs to be optimized to ensure reliable, continuous operation under industrial conditions. Despite these challenges, the redox-mediated recycling strategy represents a paradigm shift in sustainable battery recycling. By replacing bulk chemical consumption with renewable electricity and enabling simultaneous resource recovery and energy generation, this approach has the potential to redefine the economics and environmental footprint of lithium-ion battery recycling. With continued innovation and scale-up, redox-mediated processes could emerge as a transformative upcycling technology, playing a pivotal role in building a circular and low-carbon energy economy.

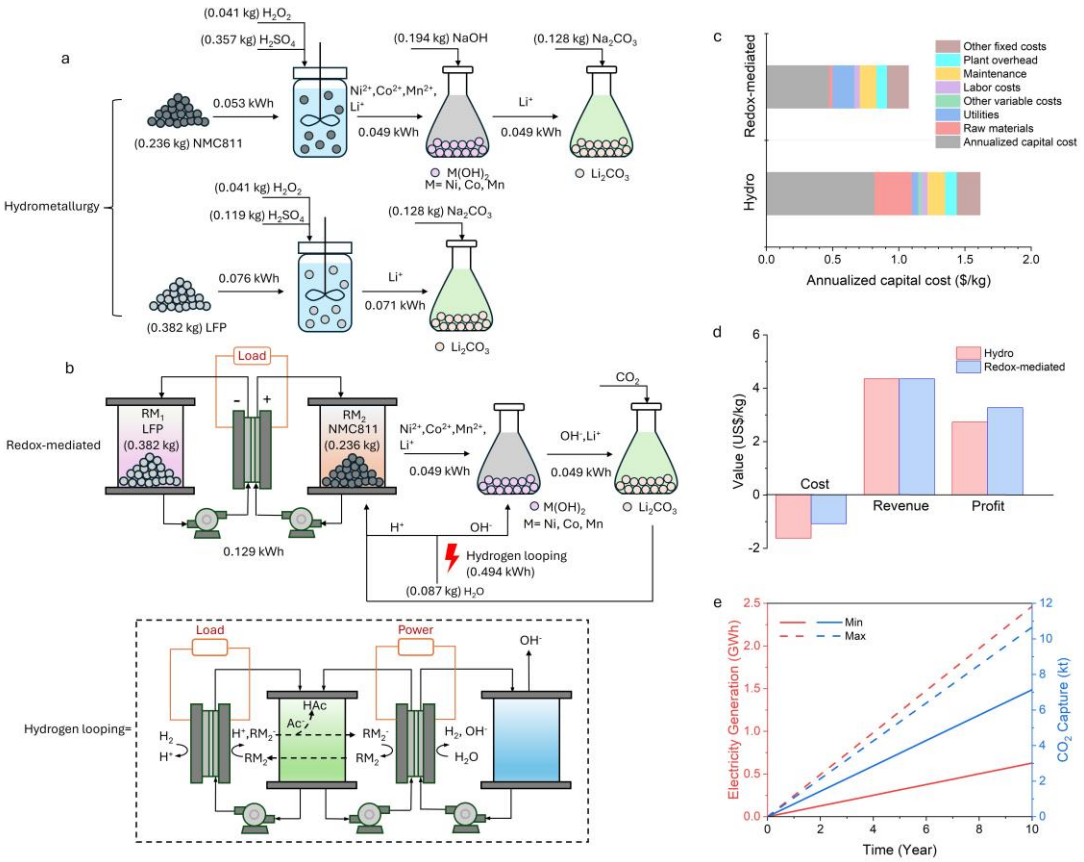

Figure 5. Techno-economic analysis of the complementary redox-mediated recycling process. a-b, Flow chart of the recycling processes with mass and energy balances of (a) hydrometallurgical recycling and (b) redox-mediated complementary recycling processes. c, Unit-cost breakdowns of hydrometallurgical and redox-mediated recycling processes. d, Cost, revenue and profit of the different recycling processes. e, Amount of generated electricity and captured CO_2 over ten years of operation, considering the utilization of actives materials in black mass, mediator durability, and hydrogen-looping efficiency.

Discussion

Here we report a complementary redox-mediated strategy for spent LIBs recycling, capable of simultaneously processing various types of spent cathode materials with electricity generation and CO_2 capture. With a redox-targeting flow cell design, spent $LiFePO_4$ and NMC/LCO are used as the anodic and cathodic feedstocks, respectively. Redox-mediated oxidative leaching of $LiFePO_4$ in the anodic compartment and reductive leaching of NMC/LCO in the cathodic compartment paired with different redox mediators generate electricity, while lithium ions are accumulated from the anolyte to the catholyte during discharge process. With optimal utilization of the spent cathode materials, the electricity generation rate is estimated to be 246 MWh per annum. Additionally, by capturing CO_2 from industrial waste gases and converting it into Li_2CO_3, the system can reduce

emissions by 1,066 tonne per annum. Further integrating a hydrogen looping for acid and base regeneration, the process establishes a sustainable, closed-loop system with zero chemical consumption. This strategy demonstrates broad applicability for recycling various spent cathode materials and shows great promise for large scale application. We anticipate that our approach can promote comprehensive sustainability while minimizing costs and environmental impact for spent LIBs recycling.

Methodes

Materials

$LiNi_{0.8}Mn_{0.1}Co_{0.1}O_2$ (NMC811), $LiFePO_4$ (LFP) and $LiCoO_2$ (LCO) were purchased from Beyond Battery and detailed specifications are available on the manufacturer's website. LiAc (99%) and Anthraquinone-2,7-disulfonic acid disodium salt (AQDS, 80%) were purchased from BLDpharm. KCl (>99%), NaOH (≥98%), LiOH (98%), HAc (≥99%), H_2SO_4 (95.0-98.0%), $BQDS{\cdot}H_2O$ (97%), $Ni(Ac)_2{\cdot}4H_2O$ (98%), $Co(Ac)_2{\cdot}4H_2O$ (≥98%), $Mn(Ac)_2{\cdot}4H_2O$ (≥99%) and $Fe_4[Fe(CN)_6]_3$ (99.3%) were purchased from Sigma-Aldrich. $Li_4Fe(CN)_6$ was prepared by reacting 2.86 g of $Fe_4[Fe(CN)_6]_3$ with 40 mL of 1 M LiOH aqueous solution for 10 h, yielding 40 mL of a yellowish 0.20 M $Li_4Fe(CN)_6$ solution with $Fe(OH)_3$ precipitate. $Li_3Fe(CN)_6$ was obtained by electrolysis of the $Li_4Fe(CN)_6$ solution.[41] THBDS was electrochemically synthesized by cycling BQDS in an electrochemical cell.[38] Nafion 115 and 212 (Dupont) membrane was purchased from Chemours.

Granule preparation

The NMC811, LFP and LCO granules in short stick shape were made by a granulation machine (Caleva Multi Lab) with NMC811, LFP and LCO powder, carbon black as a conductive additive, PVDF as a binder, and NMP as solvent at 25 ºC±1 ºC.

Electrochemical measurements

All electrochemical measurements were conducted with an Autolab electrochemical workstation (Metrohm, PGSTAT30) at 25 ºC±1 ºC. Cyclic voltammetric (CV) measurements were carried out using a three-electrode glass cell composed of a glassy carbon working electrode, a platinum plate counter electrode and an Ag/AgCl reference electrode. Open circuit potential (OCP) measurements of the equilibrium potentials of MNC811, LFP and LCO were carried out using a two-compartment glass cell composed of a working electrode (carbon paper coated with active materials) and an Ag/AgCl reference electrode. OCP measurements of the reaction kinetics of $[Fe(CN)_6]^{3-}$ mediated LFP oxidation process were carried out using a two-compartment glass cell composed of a rotating disk electrode and an Ag/AgCl reference electrode, the rotating speed for the experiments were 1000 rpm. The glassy carbon working electrode was polished with 0.3 and 0.05 μm of alumina slurry for 2 minutes and then sonicated in deionized water before every test.

Flow battery assembly

In the flow cell, Nafion 115 or 212 membranes were used to separate the catholyte and anolyte, which were soaked in supporting electrolytes overnight prior to use. Carbon felt (Mianyang Hitek Co., Ltd) was used as the electrode. Viton gasket and PTFE tubing (Cole-Parmer) were employed to build the cell. The active area of carbon felt was 5 cm^2. The flow field material was graphite. For the leaching and discharge tests of NMC811 and LCO, the $[Fe(CN)_6]^{4-}$-THBDS/NMC811(LCO) flow cells were assembled to calculate the utilization of NMC811(LCO) at various current density of 1 mA cm^{-2}, 5 mA cm^{-2} and 10 mA cm^{-2}. 15 mL 30 mM THBDS/5M HAc/1 M KCl was used as catholyte with various NMC811(LCO) granules loading (0.077 g or 1.155 g active materials) and 60 mL 0.2 M $[Fe(CN)_6]^{4-}$/2 M KAc was used as anolyte. For the spent cathode utilization tests of LFP, the $[Fe(CN)_6]^{3-}$ based symmetric flow batteries were assembled to calculate the utilization of LFP at current density of 1 mA cm^{-2}, 5 mA cm^{-2} and 10 mA cm^{-2}. 60 mL 0.1 M $Li_3Fe(CN)_6$ was used as catholyte and 15 mL 0.1 M $Li_3Fe(CN)_6$ was used as anolyte with LFP granules (0.27 g or 0.52 g LFP) loading. For the full cell tests using THBDS/$THBDS^{2+}$ as redox mediator, 15 mL 30 mM $THBDS^{2+}$/5 M HAc/1 M KCl was used as catholyte with NMC811(LCO) granules (1.15 g NMC811/LCO) loaded in the cathodic tank and 25 ml 0.2 M $Li_4Fe(CN)_6$/3 M LiAc was used as anolyte with LFP granules (1.99 g LFP) loaded in the anodic tank. The current density was 10 mA cm^{-2}. For the full cell tests using BQDS as redox mediator, 20 mL 0.1 M BQDS/1 M H_2SO_4 was used as catholyte with 0.30 g NMC811 loaded in the cathodic tank and 20 ml 0.2 M $Li_3Fe(CN)_6$/3 M LiAc was used as anolyte with 0.6 g LFP loaded in the anodic tank. The current density was 10 mA cm^{-2}. For the power tests, the battery stack was constructed with 6 single cells. The catholyte was 35 ml 0.1 M THBDS/5 M HAc/1 M KCl or 0.1 M BQDS/5 M HAc/1 M KCl or 0.1 M BQDS/1 M H_2SO_4, and the anolyte was 35 mL 0.2 M $Li_3Fe(CN)_6$/3 M LiAc. Excessive of NMC811 and LFP were loaded in the cathodic and anodic tanks for the power tests. For the full cell tests with blackmass leaching experiments. The NMC622 and LFP blackmass first reacted with THBDS and $Li_3Fe(CN)_6$ for around 3 hours, respectively. And then 10 mL reacted THBDS solution was used as catholyte and 15 mL reacted $Li_3Fe(CN)_6$ was used as anolyte, the current density was 2 mA cm^{-2}. For the stability tests of $Li_4Fe(CN)_6$, 10 ml 0.1 M $Li_4Fe(CN)_6$/3 M LiAc and 20 ml 0.1 M $K_3Fe(CN)_6$/0.02 M $K_4Fe(CN)_6$/3 M LiAc were used as catholyte and anolyte, respectively. The current density is 40 mA cm^{-2}. For the stability tests of THBDS, 15 ml 30 mM THBDS/5 M HAc and 20 ml 0.1 M $K_3Fe(CN)_6$/0.02 M $K_4Fe(CN)_6$/3 M LiAc were used as catholyte and anolyte, respectively. The current density is 10 mA cm^{-2}. For the stability tests of BQDS, 10 mL 0.1 M BQDS/1 M H_2SO_4 and 35 mL 0.05 M AQDS/1 M H_2SO_4 were used as catholyte and anolyte, respectively. The current density is 40 mA cm^{-2}. The galvanostatic measurements of flow batteries were performed with an Arbin battery tester at 25 ºC±1 ºC. No climatic/environmental chamber is used for all the experiments.

Characterizations

All the UV-vis experiments were conducted with a SHIMADZU UV-2700i spectrometer at 25 ºC±1 ºC with a fast scan speed. UV-vis spectra of the THBDS solution were recorded in situ for kinetic analysis by continuously flowing the THBDS solution through an excess of NMC811/LCO

in reaction tanks. A custom-designed spectro-electrochemical cell with 0.6 mm optical path length was connected to the outlet of the reaction tank (Figure S6). The electrolyte was 15 mL 30 mM THBDS/5 M HAc. For the operando UV-vis spectra of THBDS, it was conducted through $[Fe(CN)_6]^{4-}$-$THBDS^{2+}$ flow cells with and without MNC811/LCO loaded in the reaction tanks. A custom-designed spectro-electrochemical cell with 0.6 mm optical path length was connected to the outlet of the cathodic tank (Figure S8). The absorbance changes of THBDS were recorded during the reaction process. 20 mL 30 mM $THBDS^{2+}$/5 M HAc/1 M KCl was used as catholyte and 50 mL 0.3 M $K_4Fe(CN)_6$/0.05 M $K_3Fe(CN)_6$/2 M LiAc was used as the anolyte. NMC811/LCO granules were loaded in the cathodic tanks and the current density was 10 mA cm^{-2}. For the operando UV-vis spectra of $[Fe(CN)_6]^{3-}$, it was conducted by the $[Fe(CN)_6]^{3-/4-}$ symmetric flow cell with and without LFP granules loaded in reaction tanks. A custom-designed spectro-electrochemical cell with 0.6 mm optical path length was connected to the outlet of the anodic tank (Figure S21). The absorbance changes of $[Fe(CN)_6]^{3-}$ were recorded during the reaction process. 25 mL 0.1 M $Li_4Fe(CN)_6$/1 M LiAc was used as anolyte and 30 mL 0.4 M $K_3Fe(CN)_6$/0.05 M $K_4Fe(CN)_6$/1 M LiAc was used as the catholyte. LFP granules were loaded in the anodic tanks and the current density was 10 mA cm^{-2}.

XRD measurements were conducted on a Powder XRD Diffractometer System (Bruker D8 Advance) with a step size of 0.02º and SEM measurements were conducted on Zeiss Sigma 300. The 1H- nuclear magnetic resonance (NMR) was recorded on a BRUKER 500MHz spectrometer (magnetic field: 11.7 T). Elemental analysis was conducted on Perkin Elmer Avio 500 Inductively Coupled Plasma-Optical Emission Spectrometer. All the experiments were conducted at 25 ºC±1 ºC.

Computational methods

Geometry optimizations were performed using the B3LYP-GD3BJ/6-311G* level of theory, incorporating the SMD-water solvation model. These calculations were carried out with the Gaussian09 D01 software package on the High Performance Computing (HPC) clusters at the National University of Singapore.

Details of techno-economic analysis

Cost analysis

Materials cost is one of the most important factors of the overall recycling cost. At present, the most commercially adopted recycling method is the hydrometallurgical method, for which inorganic acids are usually used. In order to accurately calculate the cost of various reagents, we selected the presently most mature sulfuric acid system, and the reactions for the Hydro process are shown below:

For NMC-based spent cathode:

Acid leaching:

$$LiNi_xMn_yCo_zO_2 + 3H^+ + 0.5H_2O_2 \rightarrow Li^+ + 2H_2O + xNi^{2+} + yMn^{2+} + zCo^{2+} + 0.5\ O_2\ (x+y+z=1)$$

Transition metal precipitation:

$$xNi^{2+} + yMn^{2+} + zCo^{2+} + 2OH^- \rightarrow Ni_xMn_yCo_z(OH)_2 \downarrow$$

Li^+ precipitation:

$$2Li^+ + CO_3^{2-} \rightarrow Li_2CO_3 \downarrow$$

For LFP-based spent cathode:

Acid leaching:

$$2LiFePO_4 + 2H^+ + H_2O_2 \rightarrow 2Li^+ + 2H_2O + 2FePO_4$$

Li^+ precipitation:

$$2Li^+ + CO_3^{2-} \rightarrow Li_2CO_3 \downarrow$$

Here based on the EverBatt 2023 Model, we take NMC811and LFP as an example for cost analysis. Considering 1 kg of black mass contains 0.236 kg NMC811 and 0.382 kg LFP. So the H_2SO_4, H_2O_2, NaOH and Na_2CO_3 used for NMC811 spent cathode are 0.357 kg, 0.041 kg, 0.194 kg and 0.128 kg, respectively. And H_2SO_4, H_2O_2 and Na_2CO_3 used for LFP spent cathode are 0.119 kg, 0.041 kg and 0.128 kg, respectively. The overall consumption of H_2SO_4, H_2O_2, NaOH and Na_2CO_3 for 1 kg black mass are 0.476 kg, 0.082 kg, 0.194 kg and 0.256 kg.

While for the redox-mediated method, since the redox mediators are reusable, and the first step of leaching process can be described as follows:

$$LiFePO_4 + LiNi_xMn_yCo_zO_2 + 4H^+ \rightarrow 2Li^+ + FePO_4 + xNi^{2+} + yMn^{2+} + zCo^{2+} + 2H_2O\ (x+y+z=1)$$

The following transition metal and Li^+ precipitation processes are as follows:

$$xNi^{2+} + yMn^{2+} + zCo^{2+} + 2OH^- \rightarrow Ni_xMn_yCo_z(OH)_2 \downarrow$$

$$2Li^+ + CO_2 + 2OH^- \rightarrow Li_2CO_3 \downarrow + H_2O$$

Considering the whole recycling process consumes H^+ and OH^-, which are then regenerated by the hydrogen looping process using electricity (0.494 kWh/kg), the chemical cost of the complementary redox-mediated method is negligible. And the usage and cost of consumed chemicals and electricity are summarized in Table S5.

Electricity generation

Consider a recycling plant processes 10,000 tonne of black mass annually and can continuously operate for 10 years.

For THBDS-based catholyte using HAc supporting electrolyte, 1.15 g NMC-based spent cathode can generate 0.031 Wh electricity (as demonstrated in Figure 4a). So, the electricity generated per kg of NMC-based spent cathode is calculated to be:

$$Electricity_{THBDS}^{0} = \frac{0.031 \times 1000}{1.15} = 26.96\ Wh/kg$$

So over 10 years' operation, considering the hydrogen-looping efficiency (98.8%), the total generated electricity is calculated to be:

$$Electricity_{THBDS}^{total} = Electricity_{THBDS}^{0} \times 98.8\% \times 2358.24 \times 1000 \times 10 \times 10^{-6} = 628\ MWh$$

For BQDS-based catholyte using H_2SO_4 supporting electrolyte, the theoretical electricity generated per kg of NMC-based spent cathode is calculated to be:

$$Electricity_{BQDS}^{0} = V_{cell} \times C = (0.85 - 0.47) \times 0.275 \times 1000 = 104.5\ Wh/kg$$

So over 10 years' operation, the total generated electricity is calculated to be:

$$Electricity_{BQDS}^{total} = Electricity_{BQDS}^{0} \times 2358.24 \times 1000 \times 10 \times 10^{-6} = 2464\ MWh$$

CO_2 capture

Regardless of the redox mediators used in the catholyte, CO_2 capture is related to the availability of Li^+ in the solution. Assuming 100% reaction yield of active materials in the black mass, the CO_2 capture rate is calculated to be:

$$rate = \frac{2358}{320 \times 97.279} \times 44 = 3.33\ t/day$$

Over 10 years' operation, the total CO_2 captured was estimated to be:

$$CO_2^{Captured} = rate \times operation\ time = 3.33 \times 320 \times 10 = 10656\ t$$

Based on the demonstrated 67% utilization of active materials, the total CO_2 captured over a 10-year operational period is estimated at 7,140 t. Accordingly, the overall CO_2 capture is projected to range from 7,140 t to 10,656 t depending on the utilization efficiency.

Data availability

All the data generated in this study are provided in this paper and its Supplementary information file. Source data are provided with this paper.

References

1. Service, R.F. Lithium-ion battery development takes Nobel. *Science* **366**, 292-292 (2019).
2. Tian, Y. et al. Promises and Challenges of Next-Generation "Beyond Li-ion" Batteries for Electric Vehicles and Grid Decarbonization. *Chemical Reviews* **121**, 1623-1669 (2021).
3. Harper, G. et al. Recycling lithium-ion batteries from electric vehicles. *Nature* **575**, 75-86 (2019).
4. Biswal, B.K., Zhang, B., Thi Minh Tran, P., Zhang, J. & Balasubramanian, R. Recycling of spent lithium-ion batteries for a sustainable future: recent advancements. *Chemical Society Reviews* **53**, 5552-5592 (2024).
5. IEA (2022), Global Supply Chains of EV Batteries, IEA, Paris https://www.iea.org/reports/global-supply-chains-of-ev-batteries.
6. Ciez, R.E. & Whitacre, J.F. Examining different recycling processes for lithium-ion batteries. *Nature Sustainability* **2**, 148-156 (2019).
7. Yang, T., Luo, D., Yu, A. & Chen, Z. Enabling Future Closed-Loop Recycling of Spent Lithium-Ion Batteries: Direct Cathode Regeneration. *Advanced Materials* **35**, 2203218 (2023).
8. Li, Z. et al. Lithium extraction from brine through a decoupled and membrane-free electrochemical cell design. *Science* **385**, 1438-1444 (2024).
9. Fan, E. et al. Sustainable Recycling Technology for Li-Ion Batteries and Beyond: Challenges and Future Prospects. *Chemical Reviews* **120**, 7020-7063 (2020).
10. Ma, R. et al. Pathway decisions for reuse and recycling of retired lithium-ion batteries considering economic and environmental functions. *Nature Communications* **15**, 7641 (2024).
11. Makuza, B., Tian, Q., Guo, X., Chattopadhyay, K. & Yu, D. Pyrometallurgical options for recycling spent lithium-ion batteries: A comprehensive review. *Journal of Power Sources* **491**, 229622 (2021).
12. Gaines, L. The future of automotive lithium-ion battery recycling: Charting a sustainable course. *Sustainable Materials and Technologies* **1-2**, 2-7 (2014).
13. Zhang, X. et al. Innovative Application of Acid Leaching to Regenerate Li(Ni1/3Co1/3Mn1/3)O2 Cathodes from Spent Lithium-Ion Batteries. *ACS Sustainable Chemistry & Engineering* **6**, 5959-5968 (2018).
14. Yao, Y. et al. Hydrometallurgical Processes for Recycling Spent Lithium-Ion Batteries: A Critical Review. *ACS Sustainable Chemistry & Engineering* **6**, 13611-13627 (2018).
15. Wu, X. et al. Toward Circular Energy: Exploring Direct Regeneration for Lithium-Ion Battery Sustainability. *Advanced Materials* **36**, 2403818 (2024).
16. Ji, G. et al. Direct regeneration of degraded lithium-ion battery cathodes with a multifunctional organic lithium salt. *Nature Communications* **14**, 584 (2023).
17. Wang, J. et al. Sustainable upcycling of spent LiCoO2 to an ultra-stable battery cathode at high voltage. *Nature Sustainability* **6**, 797-805 (2023).
18. Mao, J. et al. Toward practical lithium-ion battery recycling: adding value, tackling circularity and recycling-oriented design. *Energy & Environmental Science* **15**, 2732-2752 (2022).
19. Natarajan, S. & Aravindan, V. Recycling Strategies for Spent Li-Ion Battery Mixed Cathodes. *ACS Energy Letters* **3**, 2101-2103 (2018).
20. Ji, G. et al. Sustainable upcycling of mixed spent cathodes to a high-voltage polyanionic cathode material. *Nature Communications* **15**, 4086 (2024).

21. Zou, H., Gratz, E., Apelian, D. & Wang, Y. A novel method to recycle mixed cathode materials for lithium ion batteries. *Green Chemistry* **15**, 1183-1191 (2013).
22. Li, L. et al. Process for recycling mixed-cathode materials from spent lithium-ion batteries and kinetics of leaching. *Waste Management* **71**, 362-371 (2018).
23. Zhou, M. et al. Single-Molecule Redox-Targeting Reactions for a pH-Neutral Aqueous Organic Redox Flow Battery. *Angewandte Chemie International Edition* **59**, 14286-14291 (2020).
24. Wang, Z. et al. Scalable Direct Recovery of Spent LiFePO4 with a Redox-Mediated Flow Cell. *ACS Energy Letters* **10**, 3064-3073 (2025).
25. Yang, T. et al. Sustainable regeneration of spent cathodes for lithium-ion and post-lithium-ion batteries. *Nature Sustainability* **7**, 776-785 (2024).
26. Zhao, L., Ren, X. & Yan, X. Assembly Induced Super-Large Red-Shifted Absorption: The Burgeoning Field of Organic Near-Infrared Materials. *CCS Chemistry* **3**, 678-693 (2021).
27. Pierpont, C.G. & Buchanan, R.M. Transition metal complexes of o-benzoquinone, o-semiquinone, and catecholate ligands. *Coordination Chemistry Reviews* **38**, 45-87 (1981).
28. Pierpont, C.G. Unique properties of transition metal quinone complexes of the MQ3 series. *Coordination Chemistry Reviews* **219-221**, 415-433 (2001).
29. Özcan, E. et al. Ultrafast excited states dynamics of metal ion complexes of the carotenoid astaxanthin. *Journal of Photochemistry and Photobiology A: Chemistry* **441**, 114737 (2023).
30. van Leeuwen, P.W.N.M. & Groeneveld, W.L. Inorganic complexes with acetic acid as the ligand. *Recueil des Travaux Chimiques des Pays-Bas* **87**, 86-96 (1968).
31. Billy, E. et al. Dissolution Mechanisms of LiNi1/3Mn1/3Co1/3O2 Positive Electrode Material from Lithium-Ion Batteries in Acid Solution. *ACS Applied Materials & Interfaces* **10**, 16424-16435 (2018).
32. Joulié, M., Billy, E., Laucournet, R. & Meyer, D. Current collectors as reducing agent to dissolve active materials of positive electrodes from Li-ion battery wastes. *Hydrometallurgy* **169**, 426-432 (2017).
33. Xuan, W., de Souza Braga, A., Korbel, C. & Chagnes, A. New insights in the leaching kinetics of cathodic materials in acidic chloride media for lithium-ion battery recycling. *Hydrometallurgy* **204**, 105705 (2021).
34. Xu, P. et al. Proton-exchange induced reactivity in layered oxides for lithium-ion batteries. *Nature Communications* **15**, 9842 (2024).
35. Meng, Z., Ma, X., Hou, J., Zheng, Y. & Wang, Y. Impurity Impacts of Recycling NMC Cathodes. *Advanced Energy Materials* **n/a**, 2405383 (2025).
36. Kim, W., Park, S., Ko, G., Lee, J. & Kwon, K. Optimizing pH conditions for impurity removal in closed-loop Li-ion battery recycling. *Chemical Engineering Journal* **475**, 146121 (2023).
37. Xu, L., Zhou, F., Kong, J., Chen, Z. & Chen, K. Synthesis of Li(Ni0.6Co0.2Mn0.2)O2 with sodium DL-lactate as an eco-friendly chelating agent and its electrochemical performances for lithium-ion batteries. *Ionics* **24**, 2261-2273 (2018).
38. Yang, B. et al. High-Performance Aqueous Organic Flow Battery with Quinone-Based Redox Couples at Both Electrodes. *Journal of The Electrochemical Society* **163**, A1442 (2016).
39. Wang, J. et al. Direct recycling of spent cathode material at ambient conditions via spontaneous lithiation. *Nature Sustainability* **7**, 1283-1293 (2024).

40. Yuan, Z. et al. Low-cost hydrocarbon membrane enables commercial-scale flow batteries for long-duration energy storage. *Joule* **6**, 884-905 (2022).
41. Yu, J., Wang, X., Zhou, M. & Wang, Q. A redox targeting-based material recycling strategy for spent lithium ion batteries. *Energy & Environmental Science* **12**, 2672-2677 (2019).

Acknowledgement

This research is supported by the National Research Foundation, Singapore, under its Competitive Research Programme (Award No.: NRF-CRP26-2021-0003 (Q.W.)), and by A*STAR under its MTC Programmatic Fund (Award No.: M24N5b0037 (Q.W.)).

Author contribution

Q.W., S.Q.H. and S.P.H. conceived the study. Q.W. supervised the work. S.Q.H. performed most of the experiments and data analysis. S.P.H. did preliminary tests. M.L. assisted with battery tests and granule synthesis. H.Z. conducted DFT calculations. X.W. advised on techno-economic analysis. M.S. conducted the NMR tests. S.Q.H. and Q.W. wrote the paper.

Competing interests

The authors declare no competing interests.

Figure 1. Schematic illustration of a sustainable redox-mediated spent LIB cathode materials recycling process. The system includes high-value metals leaching, transition metals separation, lithium recovery and base/acid regeneration. The high-value metals are extracted using a redox-targeting flow cell, where the spent cathode materials are used as the feedstock and redox active molecules serve as the mediators. The molecules shuttle between electrodes and reactor tanks, facilitating the transfer of electrons/holes through a chemical-electrochemical loop, while simultaneously generating electricity. The high-valued metals are accumulated in the catholyte during the continuous discharge process. The transition metal ions (M^{2+}) are separated via precipitation, forming metal hydroxides ($M(OH)_2$) and Li^+ captures CO_2 to produce Li_2CO_3. Both $M(OH)_2$ and Li_2CO_3 serve as precursors for synthesizing new cathode materials. To promote a sustainable recycling process with minimal chemical consumption and lower CO_2 emissions, base/acid regeneration occurs via a hydrogen looping process, where OH^- and H^+ are regenerated stepwise through a water-dissociation reaction, consuming only water. Cation-exchange membrane (CEM) was employed for all the flow cells.

Figure 2. The redox-mediated reductive leaching process of NMC811. a, CV curve of THBDS and the equilibrium potential of NMC811 in 5 M HAc. The working electrode is a glassy carbon disk and the scan rate for CV was 50 mV s^{-1}. Insert shows the molecular structure of THBDS. b,

Concentration change *vs*. concentration plot of THBQS as obtained from in situ UV-Vis measurement. The reaction is assumed to be first-order and the rate constant is determined by the slope. Insert shows the colour changes of THBDS before and after reaction. The transparent THBDS became reddish after the reaction process. c-d, Operando UV-Vis spectra of catholyte of $[Fe(CN)_6]^{4-}$/$THBDS^{2+}$ flow cells without and with NMC811 loaded in the cathodic tanks during the discharge process. e, Corresponding voltage profiles of the $[Fe(CN)_6]^{4-}$/$THBDS^{2+}$ flow cells. The current density was 10 mA cm^{-2}.

Figure 3. The redox-mediated oxidative leaching process of LFP. a, CV curve of $[Fe(CN)_6]^{3-/4-}$ and the equilibrium potential of LFP in 3 M LiAc. The working electrode is a glassy carbon disk and the scan rate for CV was 50 mV s^{-1}. b, Concentration change *vs*. concentration plot of $[Fe(CN)_6]^{3-}$ as obtained from OCP measurement. The reaction is assumed to be first-order and the rate constant is determined by the slope. c-d, Operando UV-Vis spectra of anolyte of $[Fe(CN)_6]^{3-/4-}$-based symmetric flow cells without and with LFP loaded in the anodic tanks during the discharge process. e, Corresponding voltage profiles of the $[Fe(CN)_6]^{3-/4-}$-based symmetric flow cells. The current density was 10 mA cm^{-2}.

Figure 4. Complementary redox-mediated spent cathode materials recycling. a, Voltage profile of a $[Fe(CN)_6]^{4-}$/$THBDS^{2+}$ flow cell with LFP loaded in the anodic reactor tank and NMC811 in the cathodic reactor tank. The current density is 10 mA cm^{-2} and voltage profile is plotted with IR correction. b, Concentrations of Li^{+}, Ni^{2+}, Co^{2+} and Mn^{2+} in catholyte after each step. c, SEM image of $Ni_{0.806}Mn_{0.1}Co_{0.11}(OH)_2$ with the corresponding elemental mapping results of Ni (purple), Co (green) and Mn (yellow). d, XRD pattern of the Li_2CO_3 product. e, Voltage profiles of the HER and HOR cells during the hydrogen looping processes and the corresponding pH changes of the THBDS-based electrolyte. For the HER cell, catholyte was THBDS solution and anolyte was 0.1 M NaOH solution. Pt was used as the HER catalysts. The current density was 50 mA cm^{-2}. For the HOR cell, THBDS solution was used catholyte and H_2 gas was supplied to the negative electrode. Pt/C was used as the HOR catalysts. The current density was 50 mA cm^{-2}. f, Voltage profiles of the $[Fe(CN)_6]^{4-}$/$THBDS^{2+}$ flow cell after *ex-situ* leaching process and the corresponding leaching efficiency calculated based on the discharge capacity. g, The optical image of the $[Fe(CN)_6]^{4-}$/$THBDS^{2+}$ flow cell stack constructed by six single cells with NMC811 loaded in the cathodic tank and LFP in the anodic tank. h, Power vs. current density curve of the flow cell stacks. The catholytes was 35 mL 0.1 M THBDS/5 M HAc/1 M KCl or 35 mL 0.1 M BQDS/5 M HAc/1 M KCl or 35 mL 0.1 M BQDS/H_2SO_4, and the anolyte was 35 mL 0.2 M $Li_3Fe(CN)_6$/3 M LiAc. Excessive NMC811 and LFP were loaded in the cathodic and anodic tanks, respectively.

Figure 5. Techno-economic analysis of the complementary redox-mediated recycling process. a-b, Flow chart of the recycling processes with mass and energy balances of (a) hydrometallurgical recycling and (b) redox-mediated complementary recycling processes. c, Unit-cost breakdowns of hydrometallurgical and redox-mediated recycling processes. d, Cost, revenue and profit of the different recycling processes. e, Itemized comparison of hydrometallurgical (red) and redox-mediated (blue) recycling processes.

Editorial Summary:

Prevalent recycling technologies focus on processing only one type of spent cathode material, demanding high energy input and significant chemical consumption. Here, authors present a redox-mediated flow-cell strategy to recover multiple cathode types, generating electricity during the process, with >95% metal leaching efficiency.

Peer Review Information: *Nature Communications* thanks Daesung Song and the other, anonymous, reviewer(s) for their contribution to the peer review of this work. [A peer review file is available.]